JOURNAL OF SOLID STATE CHEMISTRY 65, 331–342 (1986)

β-$NbPO_5$ and β-$TaPO_5$: Bronzoïds, Second Members of the Monophosphate Tungsten Bronze Series $(PO_2)_4(WO_3)_{2m}$

H. CHAHBOUN, D. GROULT,* M. HERVIEU, AND B. RAVEAU

Equipe Matériaux-Oxydes, Laboratoire de Cristallographie, Chimie et Physique des Solides, U.A. 251, ISMRa, 14032 Caen Cedex, France

Received November 20, 1985; in revised form March 25, 1986

The oxides β-$NbPO_5$ and β-$TaPO_5$ have been studied by X-ray diffraction and high resolution electron microscopy. They exhibit different supercells based on an orthorhombic subcell with the parameters a_0 = 11.27 Å, b_0 = 5.28 Å, c_0 = 6.62 Å. It is shown that their framework corresponds to the member m = 2 of the series of monophosphate tungsten bronzes $(PO_2)_4(WO_3)_{2m}$ with pentagonal tunnels ($MPTB_P$). The structure can thus be described as built up from ReO_3-type slabs which are two octahedra wide and connected through phosphate planes. The stability of these bronzoïds is discussed with respect to that of the $MPTB_P$ compounds. The relationships between the structures of the α and β forms of $NbPO_5$ and $TaPO_5$ are studied.

Introduction

The recent study of the P—W—O system has shown the existence of a series of oxides called monophosphate tungsten bronze with pentagonal tunnels (*1–4*) whose framework is built up from ReO_3-type slabs connected through phosphate planes. Many oxides corresponding to the general formulation $(PO_2)_4(WO_3)_{2m}$ have been isolated for integral m values ranging from m = 4 to m = 16, and many intergrowths have been observed for nonintegral m values and high m values ($m > 16$). However, the lower members, and especially the second member of the series, which would correspond to the composition PWO_5, were never observed. Several $MM'O_5$ oxides exhibit allotropic forms characterized by three-dimensional framework built up from corner-sharing MO_6 octahedra and $M'O_4$ tetrahedra. Among them, the α-form of the phosphates $MOPO_4$ (M = V, Nb, Mo) (*5–8*) belongs to the same structural family as the sulfate α-$VOSO_4$ (*9–10*) and the molybdate $VOMO_4$ (*11*). This structural form can only be obtained for $TaPO_5$ under high pressure conditions (*12*). The oxides $NbPO_5$ and $TaPO_5$ exhibit another form called β which can be synthesized at atmospheric pressure (*13*). Their X-ray powder diffraction patterns as well as their vibrational spectra (*14*) indicate that these compounds are isostructural but, so far, the real structure of this β form has not been solved. The present work deals with the structural study of β-MPO_5 (M = Nb,

* To whom correspondence should be addressed.

0022-4596/86 $3.00

Ta) based on the relationships with the monophosphate tungsten bronzes $MPTB_P$ and the other $MM'O_5$ oxides.

Experimental

Preparation of the specimens. Both compounds β-$NbPO_5$ and β-$TaPO_5$ cannot be prepared in a pure state by heating the appropriate mixture of the M_2O_5 oxide (M = Nb, Ta) and ammonium phosphate $(NH_4)_2HPO_4$ on account of the volatilization of P_2O_5 at the required temperature. Hence, they have been obtained using a method similar to that described by Levin and Roth (*13*): a mixture of M_2O_5 (M = Nb or Ta) and a large excess (5:1) of $(NH_4)_2HPO_4$ is first heated to 600°C in a platinum crucible and then to 900°C, 12 hr. After leaching with boiling water, the product is filtered, crushed, and annealed in air at 1100°C. The X-ray powder pattern of the residue agrees with that of the tetragonal α form for $NbPO_5$ and with that of the β form for $TaPO_5$ (*13*). On further heating at 1300°C, the α form of $NbPO_5$ transforms to the β form isostructural with β-$TaPO_5$. During the investigation of the system Ta_2O_5–V_2O_5–P_2O_5, it has been observed that the β-$TaPO_5$ form could be stabilized at lower temperature by addition of small amounts of V_2O_5 to the stoichiometric mixture Ta_2O_5–P_2O_5 (less than 0.2 mole V_2O_5).

Diffraction data and high resolution electron microscopy. The X-ray powder patterns used for monitoring the various chemical preparations and for the measurements of the cell constants and reflection intensities, were performed with a Philips diffractometer using copper radiation (Cu$K\alpha$ = 1.5405 Å).

The electron diffraction data used for the determination of the crystal symmetry and the reflection conditions were recorded by means of a Jeol 100CX microscope fitted with an eucentric side-entry goniometer (±60°) and operating at 120 kV. The microscopy samples were obtained from the polycrystalline sinters by crushing and dispersing in alcohol on carbon coated grids.

The HREM study was carried out with a double-tilt top-entry goniometer (±10°) with a high resolution objective lens (spherical aberration constant of 0.7 mm). The beam divergence was about 1×10^{-3} rad.

Results

Electron Diffraction Investigation

The X-ray powder diffraction patterns obtained for both compounds β-$NbPO_5$ and β-$TaPO_5$ can be indexed on the basis of a monoclinic cell as previously indicated by Levin and Roth (*12*).

However, the systematic investigation of numerous samples by electron diffraction did not allow it as the only possibility. It appeared indeed that most of the crystals were characterized by a superstructure based on a distorted orthorhombic subcell with the following parameters: a_0 = 11.27 Å, b_0 = 5.28 Å, c_0 = 6.62 Å and the limited reflections ($0kl$): $k + 1 = 2n$, ($hk0$): $h = 2n$ leading to the possible space groups *Pnma* and $Pn2_1a$. It is worthy of note here that such unit cell dimensions have been found by Chernorukov *et al.* (*15*) for $TaPO_5$ specimens obtained under soft chemical conditions, i.e., by thermal dehydration of the hydrate $TaPO_5 \cdot H_2O$ at 300°C.

According to our electron diffraction study, it must be pointed out that the intensity of the superstructure reflections varied from one crystal to another. The true cell constants were determined by exploring the whole three-dimensional reciprocal lattice by taking numerous sections through it.

Several supercells were thus characterized, corresponding to a doubling of c or/and a parameters and a slight distortion of the orthorhombic subcell. The main super-

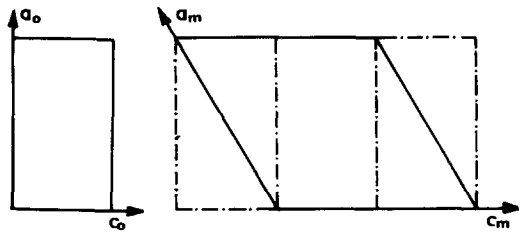

FIG. 1. Geometrical relations between the orthorhombic subcell and the monoclinic supercell of β-MPO_5 compounds (M = Nb, Ta).

cell, more often encountered, was monoclinic with the following parameters:

$$a_m = a_0 (\sin \beta)^{-1} = 13.10 \text{ Å}$$
$$b_m = b_0 = 5.28 \text{ Å}$$
$$c_m = 2c_0 = 13.24 \text{ Å}$$
$$\beta = 120°43.$$

Figure 1 shows the geometrical relationships between the orthorhombic subcell and the monoclinic supercell.

The corresponding distortion of the orthorhombic subcell is about 0°22. Reflections $h0l$ and $0k0$ are systematically absent for $l = 2n + 1$ and $k = 2n + 1$, respectively, involving the monoclinic space group $P2_1/c$.

Figure 2 illustrates the reciprocal planes (100), (010), and (201) of the supercell. The superlattice spots are clearly visible on Figs. 2a and c. The corresponding section observed for a single crystal showing weakest spots is given as an example by Fig. 3, for (100) reciprocal plane.

Besides this monoclinic supercell, three other ones, noted O_2—O_3 and O_4 because they exhibited an orthorhombic symmetry, have been identified (Fig. 4). They are characterized, respectively, by the cell-constants:

$$a_2 = 2a_0, b_2 = b_0, c_2 = 2c_0 \quad \text{for } O_2$$
$$a_3 = 2a_0, b_3 = b_0, c_3 = c_0 \quad \text{for } O_3$$
$$a_4 = a_0, \quad b_4 = b_0, c_4 = 2c_0 \quad \text{for } O_4$$

Furthermore some crystals showed more complex distortion such as the one pictured in Fig. 5: the angle between $|010|^*$ and $|\bar{1}01|^*$ directions of the monoclinic supercell appeared clearly different from 90°.

Another important feature which should be outlined is the rapid decrease and then the disappearance of the extra-spots when the intensity of the electron beam is increased. Some examples are given in Fig. 6.

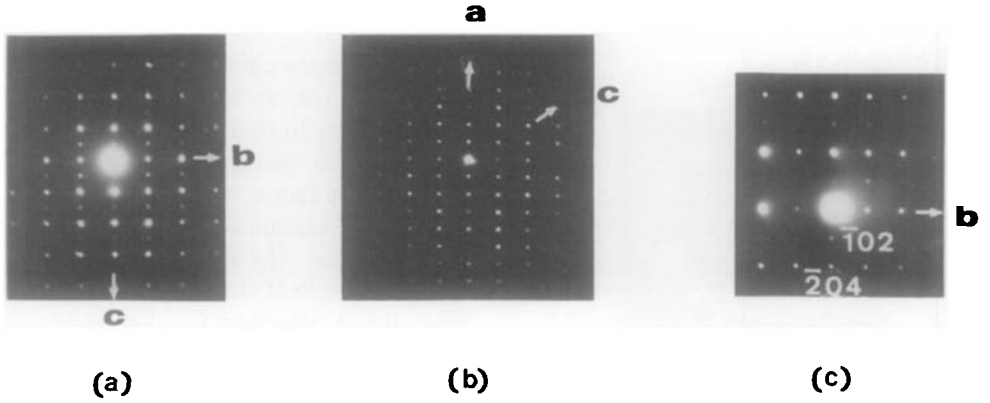

FIG. 2. Reciprocal planes (100), (010), and (201) of the supercell. ($0k0$ and $00l$ spots with k and $l \neq 2n$ appear by multiple diffraction phenomena). They correspond, respectively, to the $(\bar{1}01)$, (010), and (001) of the subcell.

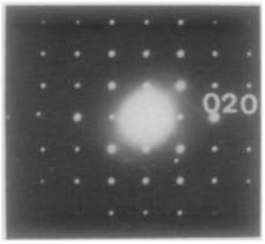

FIG. 3. Reciprocal plane (100) where the extra spots are very weak.

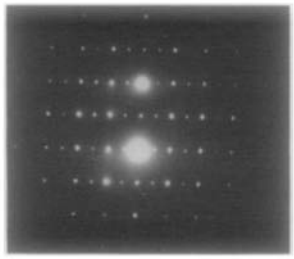

FIG. 5. ED pattern of a distorted microcrystal.

Determination of the Structural Model from the X-Ray Powder Data

The comparison of the cell-constants of the orthorhombic subcell with those which can be deduced from the equations previously established (*3*) for the monophosphate tungsten bronzes $(PO_2)_4(WO_3)_{2m}$ with pentagonal tunnels, led us to assume that β-$NbPO_5$ and β-$TaPO_5$ should correspond to the member $m = 2$ of the series. Its parameters are indeed related to those of the ReO_3-type structure in the following way:

$$a_0 \simeq 4.9 + 3.8\ m \cos 35° = 11.1\ \text{Å} \quad \text{for } m = 2$$

$$b_0 \simeq a_{ReO_3}\sqrt{2} = 5.3\ \text{Å}$$

$$c_0 \simeq a_{ReO_3}\sqrt{3} = 6.6\ \text{Å}.$$

In such an assumption a structural model can be derived from that of $P_4W_8O_{32}$ ($m = 4$) as sketched in Fig. 7.

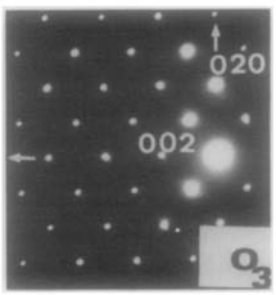

FIG. 4. Electron diffraction pattern of (100)* plane of O_3. ($b_3 = b_0$; $c_3 = c_0$) with the limited reflections $0kl$: $k + 1 = 2n$.

In order to verify this model, and especially the positions of the heavy ions, structure factor calculations were carried out from the X-ray powder diffraction data obtained for β-$TaPO_5$.

The lattice parameters were refined by use of a least-squares program. They have been listed in Table I. The X-ray reflection intensities were measured by means of a planimeter and entered in a computer program taking into account the overlapping reflections: 40 observed reflections were used. In the refinement, the atomic scattering factor for Ta^{5+}, P, and O^{2-} given by Cromer and Waber were corrected for the anomalous dispersion.

In a first step, calculations were carried out in the orthorhombic subcell with the space group *Pnma*. The refinement did not allow to lower the discrepancy factor less than 0.11. In order to confirm the model, structure factor calculations were then performed in the actual cell with the space group $P2_1/c$. In that case, all the atoms being placed in the general position 4(*e*), the discrepancy factor was reduced to 0.075 by refining the atomic coordinates of the Ta, P, and O atoms. The final atomic parameters given in Table II do not differ significantly from those obtained for the orthorhombic subcell. In the same way, the lowering of the discrepancy factor cannot be considered as significant with respect to the Cruickshank *R*-factor test. Nevertheless, it seems more convenient to preserve the

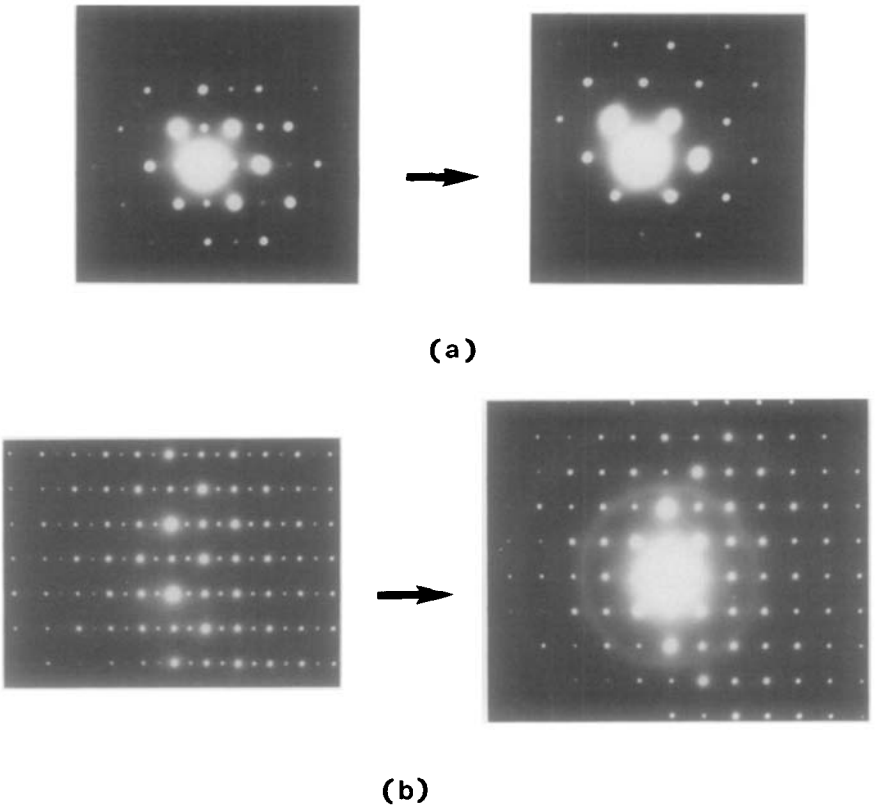

FIG. 6. Two examples of the variation of the extra-spots intensity with the increase of the intensity of the electron beam; the transitions are: (a) $|\bar{2}0\bar{1}|_M \rightarrow |100|_0$ and (b) $|100|_M \rightarrow |\bar{1}01|_0$.

space group $P2_1/c$ owing to the fact that the monoclinic supercell is, by far, the most current form which is observed by electron diffraction whereas the orthorhombic subcell is very rarely encountered. The observed and calculated values of the intensities have been listed in Table III and selected atomic distances in Table IV. The

TABLE I

UNIT CELL DIMENSIONS OF THE OXIDES β-$TaPO_5$ AND β-$NbPO_5$

Compound	Cell symmetry	Lattice parameters						Reference
		a (Å)	b (Å)	c (Å)	(°)	d_{obs}	d_{calc}	
β-$TaPO_5$	Monoclinic supercell	13.07(1)	5.281(4)	13.24(1)	120°25′ ± 4′	4.86 ± 0.05	4.92(Z = 8)	This work
β-$NbPO_5$		13.064(5)	5.283(2)	13.240(4)	120°13′ ± 2′	3.40 ± 0.02	3.43(Z = 8)	This work
β-$TaPO_5$	Orthorhombic subcell	11.27	5.281	6.62	90	—	—	This work
β-$NbPO_5$		11.262	5.283	6.620	90	—	—	This work
β-$TaPO_5$	Orthorhombic cell	11.27	5.28	6.66	90	—	—	Chernorukov *et al.* (*15*)
β-$TaPO_5$	Monoclinic cell	11.272(1)	5.281(1)	6.621(1)	90°13′ ± 1′	—	4.920(Z = 4)	Levin *et al.* (*13*)
β-$NbPO_5$		11.257(2)	5.276(1)	6.606(1)	90°17′ ± 1′	—	3.452(Z = 4)	Levin *et al.* (*13*)

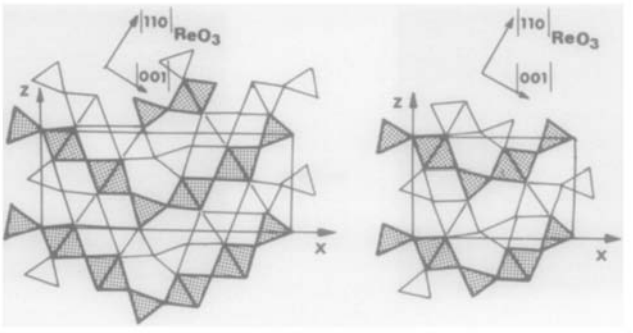

FIG. 7. Idealized drawing showing the links between the WO_6 octahedra and the PO_4 tetrahedra viewed along the *b* axis of the orthorhombic cell of the $MPTB_P$'s: (a) corresponds to the term $m = 4$ ($P_4W_8O_{32}$) and (b) to the hypothetical term $m = 2$ ($P_4W_4O_{20}$) of the series.

numbering scheme used is shown in Fig. 8. Similar results have been obtained for β-$NbPO_5$.

High Resolution Electron Microscopy Study

In order to verify the arrangement of the atoms in these oxides, a HREM study has been undertaken. β-$NbPO_5$ crystals were especially observed because they have the best transparency through the electron beam.

Thin regions of the crystal were aligned to obtain (*h0l*) reciprocal lattice sections, image astigmatism being corrected by observing the granularity of the support carbon film. Images were recorded by using an objective aperture with a radius of 0.55 $Å^{-1}$ in the reciprocal space. Simulated images were calculated using the multislice methods and programs written by Skarnulis *et al.* (*16*).

Figure 9 shows a typical low magnification image with the corresponding electron diffraction pattern in the inset, obtained for

TABLE II

FINAL ATOMIC PARAMETERS FOR β-$TaPO_5$

Atom	*x*	*y*	*z*	*B* (Å)²
Ta(1)	0.4323(6)	0.248(1)	0.3007(9)	0.15(5)
Ta(2)	0.9389(7)	0.249(1)	0.1327(7)	0.15(5)
P(1)	0.150(2)	0.25	0.053(2)	1.
P(2)	0.652(3)	0.25	0.084(2)	1.
O(1)	0.0	0.0	0.25	1.
O(2)	0.50	0.50	0.25	1.
O(3)	0.878(5)	0.0	0.016(6)	1.
O(4)	0.878(6)	0.50	0.018(7)	1.
O(5)	0.378(5)	0.50	0.377(8)	1.
O(6)	0.377(5)	0.0	0.377(7)	1.
O(7)	0.787(5)	0.25	0.133(4)	1.
O(8)	0.279(5)	0.25	0.154(4)	1.
O(9)	0.597(5)	0.25	0.452(4)	1.
O(10)	0.078(5)	0.25	0.117(5)	1.

Note. The number in parentheses represents the error in the last digit. $R_I = \Sigma|I_0 - I_c|/\Sigma I_0 = 0.075$.

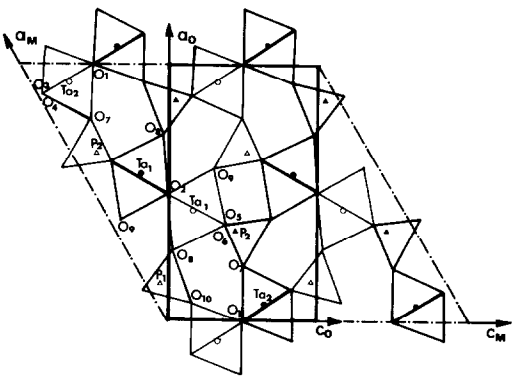

FIG. 8. Projection of the structure of β-$TaPO_5$ onto (010).

TABLE III

OBSERVED AND CALCULATED INTENSITIES FOR β-$TaPO_5$

$h\,k\,l$	I_{obs}	I_{calc}	$h\,k\,l$	I_{obs}	I_{calc}	$h\,k\,l$	I_{obs}	I_{calc}
0 0 $\bar{2}$			2 0 $\bar{6}$			2 3 2		
2 0 $\bar{2}$	81.56	84.74	4 0 $\bar{6}$			2 3 0		
2 0 0			3 2 0	16.31	12.11	2 2 $\bar{6}$		
1 0 $\bar{2}$	86.88	85.07	2 0 4			4 2 $\bar{6}$	33.33	32.99
3 0 $\bar{2}$			6 0 $\bar{4}$			2 2 4		
1 1 $\bar{2}$	100.00	121.69	2 2 4			6 2 $\bar{4}$		
0 1 2			1 0 $\bar{6}$			4 2 2		
2 1 $\bar{2}$	81.91	80.48	5 0 $\bar{6}$	6.38	4.48	1 3 2		
2 1 0			2 2 2			3 3 $\bar{2}$	12.00	8.13
1 1 2			4 2 $\bar{2}$			5 2 $\bar{6}$		
3 1 $\bar{2}$	67.02	66.49	3 1 $\bar{6}$			6 0 2		
2 0 $\bar{4}$			1 2 $\bar{4}$	8.51	9.30	8 0 $\bar{2}$		
2 0 2	18.09	19.26	3 2 $\bar{4}$			3 1 $\bar{8}$	14.54	13.73
4 0 $\bar{2}$			2 1 $\bar{6}$			5 1 $\bar{8}$		
3 1 0			4 1 $\bar{6}$			4 1 4		
0 0 4	12.77	10.64	2 1 4	12.77	14.90	8 1 $\bar{4}$		
4 0 $\bar{4}$			6 1 $\bar{4}$			0 2 6		
2 1 2	22.50	21.04	4 1 2			6 2 $\bar{6}$		
4 1 $\bar{2}$			6 1 $\bar{2}$			7 1 0	11.00	10.69
1 1 $\bar{4}$	52.13	49.87	0 2 4			1 3 $\bar{4}$		
3 1 $\bar{4}$			4 2 $\bar{4}$	15.25	13.67	3 3 $\bar{4}$		
0 2 0	26.24	24.54	4 2 0			6 2 0		
3 0 2			6 0 0			3 2 4		
5 0 $\bar{2}$	23.05	25.44	3 0 4			7 2 $\bar{4}$	17.00	15.82
1 2 0			7 0 $\bar{4}$	36.88	35.98	2 1 $\bar{8}$		
0 1 4			3 2 2			6 1 $\bar{8}$		
4 1 $\bar{4}$			5 2 $\bar{2}$			1 0 $\bar{8}$		
4 1 0	62.06	63.67	1 2 4			7 0 $\bar{8}$	27.00	23.13
1 0 4			5 2 $\bar{4}$	28.00	27.40	2 1 6		
5 0 $\bar{4}$			5 0 2			8 1 $\bar{6}$		
0 2 2			7 0 $\bar{2}$			6 1 2		
2 2 $\bar{2}$	12.41	13.08	0 1 6	30.00	28.84	8 1 $\bar{2}$		
2 2 0			6 1 $\bar{6}$			0 3 4		
5 0 0			6 1 0			4 3 $\bar{4}$	17.60	18.15
1 2 2			3 1 4	9.93	11.34	4 3 0		
3 2 $\bar{2}$	18.09	13.27	7 1 $\bar{4}$			5 2 2		
1 1 4			5 2 0			7 2 $\bar{2}$		
5 1 $\bar{4}$			5 1 2	22.70	23.67	8 1 0		
			7 1 $\bar{2}$			2 3 4		
			1 3 $\bar{2}$			2 2 $\bar{8}$	4.61	5.92
						6 2 $\bar{8}$		
						4 3 2		
						2 2 6		

β-$NbPO_5$ samples. The microcrystals appear quite perfect, without any defect contrary to those observed in the monophosphate tungsten bronzes for high m values (*3–4*). Figure 10a represents an enlargement of a part of Fig. 9 (the edge of the crystal). The important contrast features are the white blobs arranged in zigzag rows,

TABLE IV

SELECTED INTERATOMIC DISTANCES (Å) FOR β-$TaPO_5$

Ta-octahedra		P-tetrahedra	
|Ta(1)—O_6|		|P(1)—O_4|	
Ta(1)—O(2)	1.89(1) × 2	P(1)—O(3)	1.54(4) × 1
Ta(1)—O(5)	2.00(8) × 1	P(1)—O(4)	1.55(5) × 1
Ta(1)—O(6)	2.00(7) × 1	P(1)—O(8)	1.53(5) × 1
Ta(1)—O(8)	1.96(4) × 1	P(1)—O(10)	1.55(8) × 1
Ta(1)—O(9)	2.07(4) × 1		
⟨Ta(1)—O⟩ = 1.97 ± 0.04 Å		⟨P(1)—O⟩ = 1.54 ± 0.05 Å	
|Ta(2)—O_6|		|P(2)—O_4|	
Ta(2)—O(1)	1.88(1) × 2	P(2)—O(5)	1.54(6) × 1
Ta(2)—O(3)	1.88(5) × 1	P(2)—O(6)	1.53(5) × 1
Ta(2)—O(4)	1.86(5) × 1	P(2)—O(7)	1.54(7) × 1
Ta(2)—O(7)	1.99(7) × 1	P(2)—O(9)	1.52(5) × 1
Ta(2)—O(10)	1.93(7) × 1		
⟨Ta(2)—O⟩ = 1.90 ± 0.04 Å		⟨P(2)—O⟩ = 1.53 ± 0.05 Å	

parallel to the c axis. Two blob spacings are about 3.6 Å in one row and 5.8 Å from one row to the other. Between the rows, lines of dark intensity, in herring-bone pattern, are separated by broad grey lines. The atomic coordinates obtained from X-ray calculations were used for computer simulation of the images.

Calculations were carried out for various crystal thicknesses and defocus values. The computed images show a good correspondence between white blob position and the empty pentagonal tunnels for $\Delta f \sim 500$ Å and $20 < t < 50$ Å, whereas the broad grey lines correspond to the rhombic tunnels. For example, Figs. 10a–c compare the experimental image (a) with the simulated one (b) and the structural model (c) ($\Delta f = -500$ Å and $t = 26.4$ Å).

Figure 11 illustrates a feature commonly encountered in the samples; it corresponds to the existence of amorphous zones on the edges of the microcrystals. These areas exhibit various widths and shapes, as seen on this micrograph: on the left side the crystal-

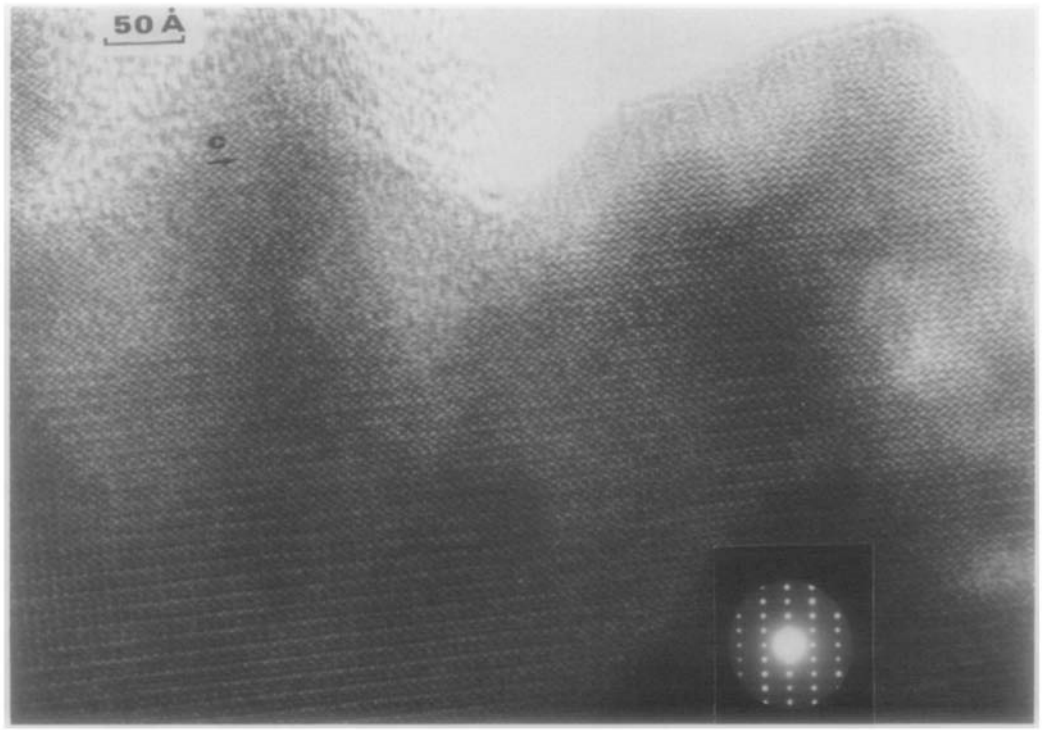

FIG. 9. Low magnification image (|010|) obtained for β-$NbPO_5$.

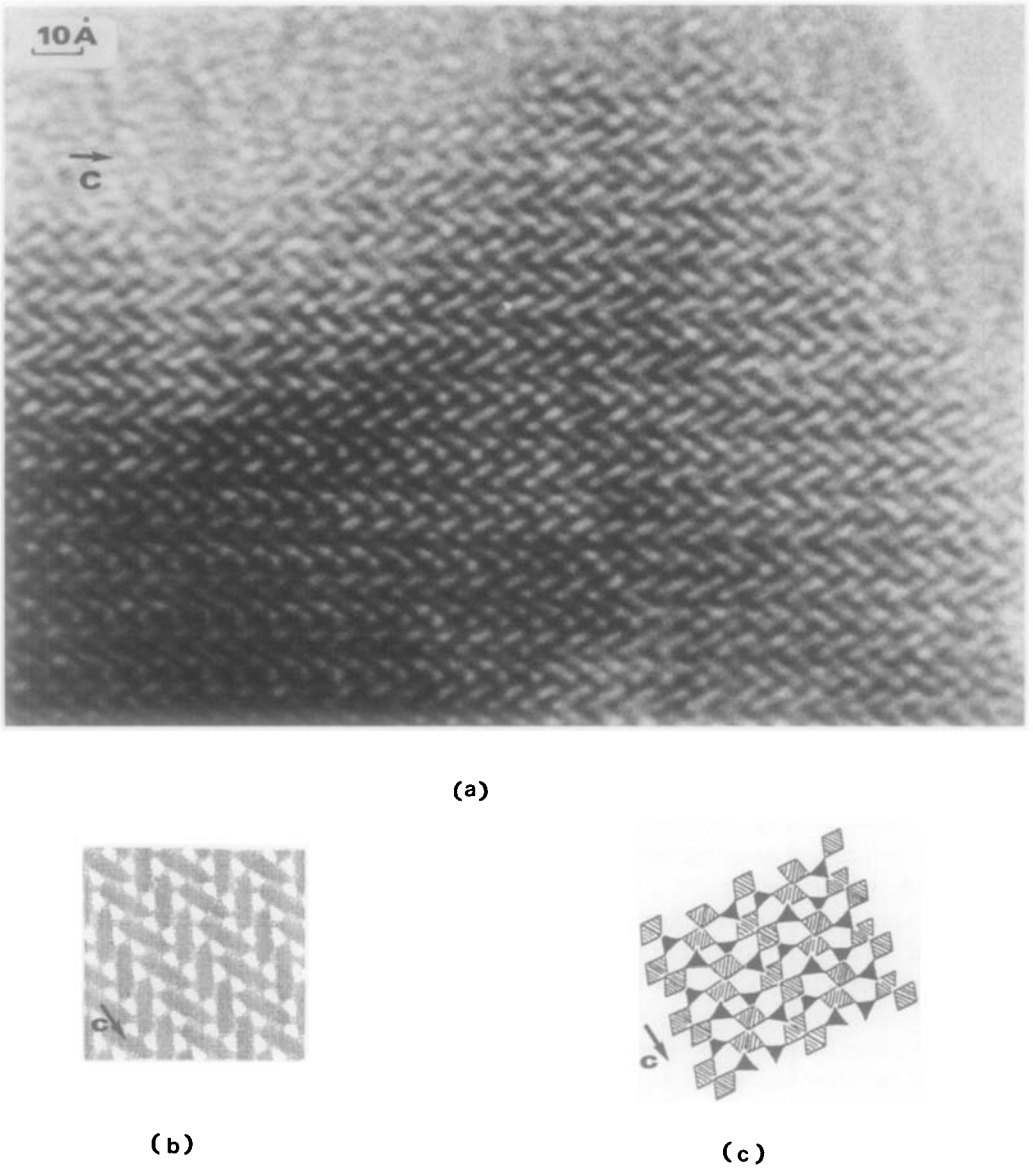

FIG. 10. (a) High resolution image (|010|); (b) calculated image for $\Delta f = -500$ Å and $t = 26.4$ Å; (c) structural model.

line zone stops in an aleatory way to give rise to an amorphous area ~450° width. On the right side, the disturbed zone (~250 Å width) is parallel to the edge of the microcrystal (it should be noted that in the latter, broad fringes of about 5.6 Å are clearly visible).

Discussion

The atmospheric pressure form β-$TaPO_5$ and the high temperature form β-$NbPO_5$ correspond to the second members of the monophosphate tungsten bronze series $MPTB_P$ $(PO_2)_4(WO_3)_{2m}$. Thus, their struc-

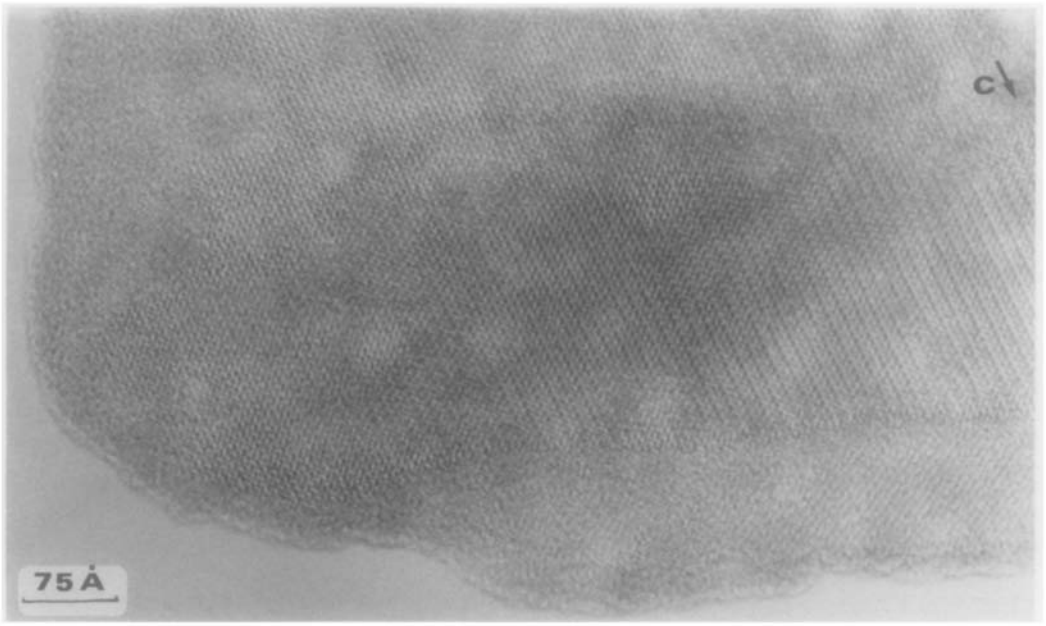

FIG. 11. Low resolution image showing the existence of amorphous zones in the microcrystals.

ture can be described as built up from narrow ReO_3-type slabs connected through phosphate planes (Fig. 8). This mixed framework delimits pentagonal tunnels running along b, which are empty.

These oxides are the smallest m-members which have been isolated up to the present: the ReO_3-type slabs are two octahedra wide along $|14\bar{1}|_m$, i.e., one octahedron wide along $|101|_m$. It is worth noting that such a member has not been observed for M = W. This can be explained by the fact that the very narrow ReO_3-type slabs are much less easily connected through PO_4 tetrahedra which are rather rigid. Consequently, a greater distortion of the framework and especially of the octahedra is necessary. This distortion is not compatible with the $5d^1$ character of W(V), in the hypothetical oxide W^VPO_5: it has indeed been observed in the A_xWO_3 HTB's (*17*) that the symmetry of the WO_6 octahedra increases with the amount of W(V), in agreement with the electronic delocalization. Thus, it appears that bronzoïds characterized by nd^0 ions in octahedral coordination such as niobium or tantalum should be favored at least for low m members.

The greater distortion of the framework of these bronzoïds with respect to the phosphate tungsten bronzes is confirmed by the fact that the most symmetric orthorhombic cell can only be stabilized for samples prepared under soft chemical conditions (*15*). In contrast, high thermal conditions induce various distortions which lead to a great variety of superstructures as shown by electron diffraction. The understanding of such distortions would necessitate a more accurate investigation from a single crystal study.

The transition from the atmospheric pressure form β-$TaPO_5$ to the high pressure form α-$TaOPO_4$ is in agreement with a 16% decrease in volume per formula as previously outlined by Longo *et al.* (*12*). The structural relationships between the two allotropic form α and β-MPO_5 (M = Nb, Ta) can be understood by considering an intermediate structural type belonging to the

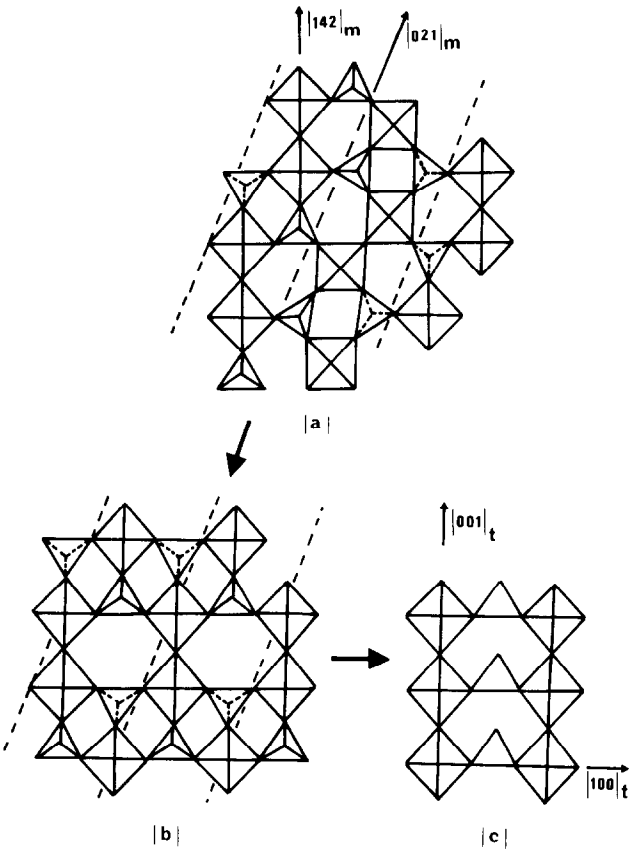

FIG. 12. Relationships between the mixed slabs of TaO_6 octahedra and PO_4 tetrahedra used to describe the structure of β-$TaPO_5$ (a), the hypothetical form β′-$TaPO_5$ (b), and α-$TaOPO_4$ (c).

monophosphate tungsten bronze series $MPTB_H$ with hexagonal tunnels (*18, 19*). The structure of β-$TaPO_5$, second member of the $MPTB_P$'s, can indeed be described in terms of two octahedra-wide ReO_3-type slabs bordered by PO_4 tetrahedra (Fig. 12a). The rotation of one slab out of two around the $|021|_m$ direction leads to a second hypothetical form β′-$TaPO_5$ (Fig. 12b) whose framework corresponds to the second member of the $MPTB_H$'s, $A_x(PO_2)_4(WO_3)_{2m}$ (A = K, Na). This latter structure is closely related to the tetragonal α-$MOPO_4$-type structure (M = V, Nb, Ta, Mo). Both structures can be described from double files of corner-sharing octahedra and tetrahedra in which one $|MO_6|$ octahedron alternates with one $|PO_4|$ tetrahedron. These double chains are parallel to the $|100|_T$ direction of the tetragonal cell of α-$MOPO_4$ (Fig. 12c). The hypothetical β-$TaPO_5$ double chains can thus be deduced from the α-$TaPO_5$ ones by a simple rotation: in one single chain the tetrahedra are rotated of 45° around the $|100|_T$ direction whereas in the second single chain, they are rotated in the same way but in the opposite direction. The three-dimensional frameworks of each structural type is then built up by association of these double chains through the corners of their polyhedra. One double chain out of two is translated of $a_T/2$ in the hypothetical β′ form with respect to the α-$TaPO_5$ form. Thus it is clear that β-$TaPO_5$ exhibits close relationships with the α-$TaPO_5$ structure. The fact that the β′ form does not exist is

easily explained by the existence of hexagonal tunnels which could be empty; the presence of ions such as sodium or potassium should be necessary to stabilize this structure as previously observed for the $MPTB_H$'s (*18–19*).

Despite the rather low accuracy about the oxygen positions in β-$TaPO_5$, the location of tantalum in its octahedron appears somewhat different from that in α-$TaPO_5$ (*12*).

While in α-$TaPO_5$ the tantalum ion is essentially octahedrally coordinated to four oxygens at 1.970 Å, one at 1.786 Å and the last at 2.215 Å implying the formula $TaOPO_4$ usually adopted for this class of compounds, the Ta–O distances calculated in the β form (Table IV) are more closely grouped in both octahedra $|Ta_{(1)}O_6|$ and $|Ta_{(2)}O_6|$. They are consistent with the differences observed between the vibrational spectra of the two forms (*14*).

On the contrary, the phosphate group is as regular as in α-$TaPO_5$, with average P–O distances of 1.54 and 1.53 Å in good agreement with those found in α-$NbOPO_4$ (1.53 Å) or $VOPO_4$ (1.54 Å) and normal orthophosphates (1.53 Å).

References

1. J. P. Giroult, M. Goreaud, Ph. Labbe, and B. Raveau, *Acta Crystallogr. Sect. B* **37,** 2139 (1981).
2. A Benmoussa, Ph. Labbe, D. Groult, and B. Raveau, *J. Solid State Chem.* **44,** 318 (1982).
3. B. Domenges, F. Studer, and B. Raveau, *Mater. Res. Bull.* **18,** 669 (1983).
4. B. Domenges, M. Hervieu, B. Raveau, and R. J. D. Tilley, *J. Solid State Chem.* **54,** 10 (1984).
5. B. Jordan and C. Calvo, *Canad. J. Chem.* **51,** 2621 (1973).
6. E. Bordes, E. Courtine, and G. Pannetier, *Ann. Chim.* **8,** 105 (1973).
7. J. M. Longo and P. Kierkegaard, *Acta Chem. Scand.* **20,** 72 (1966).
8. P. Kierkegaard and M. Westerlund, *Acta Chem. Scand.* **18,** 2217 (1964).
9. G. Ladwig, *Z. Anorg. Allg. Chem.* **365,** 225 (1969).
10. J. M. Longo and R. J. Arnott, *J. Solid State Chem.* **1,** 394 (1970).
11. A. A. Heick and L. Kihlborg, *Acta Chem. Scand.* **20,** 722 (1966).
12. J. M. Longo, J. W. Pierce, and J. A. Kafalas, *Mater. Res. Bull.* **6,** 1157 (1971).
13. E. M. Levin and R. S. Roth, *J. Solid State Chem.* **2,** 250 (1970).
14. G. T. Stranford and R. A. Condrate, Sr., *J. Mater. Sci. Lett.* **3,** 303 (1984).
15. N. G. Chernorukov, N. P. Egorov, E. V. Shitova, and Yu. I. Chigirinskii, *Russ. J. Inorg. Chem.* **26,** 1454 (1981).
16. A. J. Skarnulis, E. Summerville, and L. Eyring, *J. Solid State Chem.* **23,** 59 (1978).
17. Ph. Labbe, M. Goreaud, B. Raveau and J. C. Monier, *Acta Crystallogr. Sect. B* **34,** 1433 (1978); **35,** 1557 (1979).
18. J. P. Giroult, M. Goreaud, Ph. Labbe, and B. Raveau, *J. Solid State Chem.* **44,** 407 (1982).
19. A. Benmoussa, D. Groult, Ph. Labbe, and B. Raveau, *Acta Crystallogr. Sect. C* **40,** 573 (1984).